ORIGINAL RESEARCH

Polyallylamine Hydrochloride-Modified Bovine Serum Albumin Nanoparticles Loaded with α-Solanine for Chemotherapy of Pancreatic Cancer

Zhengde Wen[1,2,*], Shan Luo[2,3,*], Juntao Liu[4], Yufan Huang[4], Gang Chen[1], Huajie Cai [1]

[1]Department of Surgery, The First Affiliated Hospital of Wenzhou Medical University, Wenzhou, Zhejiang, People's Republic of China; [2]Wenzhou Key Laboratory of Perioperative Medicine, The First Affiliated Hospital of Wenzhou Medical University, Wenzhou, Zhejiang, People's Republic of China; [3]Department of Anaesthesia, The First Affiliated Hospital of Wenzhou Medical University, Wenzhou, Zhejiang, People's Republic of China; [4]Wenzhou Medical University, Wenzhou, Zhejiang, People's Republic of China

*These authors contributed equally to this work

Correspondence: Huajie Cai; Gang Chen, Email chjwzmu@163.com; qwechen1119@163.com

Introduction: α-Solanine (α-Sol) shows promise for pancreatic cancer (PC) treatment by inhibiting PC cell proliferation, migration, and invasion. However, its clinical application is hindered by poor tumor targeting, significant toxicity, and undesirable pharmacokinetics. To address these issues, this study developed a nanoparticle delivery system (PBSO NPs) using bovine serum albumin as a carrier, with polyallylamine hydrochloride surface modification to enhance α-Sol delivery.

Methods: PBSO NPs were characterized using transmission electron microscopy, dynamic light scattering, nanoparticle size analyzers, and Fourier-transform infrared spectroscopy. Their in vitro drug release profile and cellular uptake capabilities were evaluated. Furthermore, in vitro experiments were conducted using mouse pancreatic cancer cells (Panc02) to investigate the effects of PBSO NPs on Panc02 cell viability, migration, invasion, and apoptosis. Additionally, a pancreatic cancer xenograft tumor model was established for in vivo experiments to explore the impact of PBSO NPs on tumor growth.

Results: This study successfully developed PBSO NPs with favorable morphology and physiological stability, capable of enhancing cellular uptake. In vitro experiments demonstrated that PBSO NPs significantly inhibited the viability, migration, and invasion of Panc02 cells while promoting apoptosis. Moreover, PBSO NPs enhanced the inhibitory effects of α-Sol on Panc02 cells. In vivo experiments further confirmed that PBSO NPs improved the therapeutic efficacy of α-Sol against PC while partially reducing its toxicity. Additionally, PBSO NPs exhibited good biocompatibility.

Discussion: PBSO NPs enhance the therapeutic efficacy of α-Sol against PC by inhibiting the viability, migration, and invasion of PC cells while promoting apoptosis, thereby suppressing the progression of PC. This provides a promising therapeutic strategy for pancreatic cancer treatment.

Keywords: pancreatic cancer, α-solanine, bovine serum albumin, polyallylamine hydrochloride, apoptosis

Introduction

Pancreatic cancer (PC) is widely regarded as the "king of cancers",[1] a fatal and aggressive malignant tumor,[2] characterized by the growth of malignant cells within the pancreatic tissue.[3] PC is known for its high malignancy and early metastasis.[4] As a gastrointestinal cancer, PC progresses rapidly, and its early symptoms are often subtle or atypical, resulting in approximately 80% to 85% of patients being diagnosed at an advanced stage, when curative treatment is nearly impossible.[1] This late diagnosis is one of the main reasons for the high mortality rate of PC.[5] Furthermore, due to the location of PC near the stomach, rectum, and small intestine, surgical treatment is clinically challenging, leading to poor prognosis, with a 5-year survival rate of only 7.2%.[4] A disease-mortality model predicts that by 2040, the global incidence of PC will reach 6.093 (95% CI 5.47–6.786) per 100,000, with a higher risk in women.[6] Although survival rates for many cancers have significantly improved, the survival rate for PC patients remains largely unchanged. PC not

only exacerbates the economic burden on individuals and families but also poses a significant threat to public health.[7] Currently, chemotherapy remains the primary treatment for PC. Gemcitabine, as the first-line standard treatment for advanced pancreatic cancer, can improve survival rates but often induces resistance, limiting its efficacy. In recent years, the combination regimen FOLFIRINOX (comprising 5-fluorouracil (5-FU), leucovorin, irinotecan, and oxaliplatin) has become the gold standard for pancreatic cancer treatment, significantly extending overall survival in patients. However, its high toxicity limits its application in clinical practice.[8] Therefore, there is an urgent need to develop more effective innovative therapeutic strategies to improve the survival outcomes of PC patients.

Natural products are chemical substances produced by living organisms that possess pharmacological or biological activities, and they play an important role in the treatment of human diseases. It is estimated that approximately 80% of the drugs approved for cancer chemotherapy are derived from natural compounds [9]. Solanum nigrum L. (commonly known as black nightshade) is one of the commonly used traditional herbal medicines in clinical practice for cancer treatment. Studies have shown that its extracts exhibit significant anticancer properties.[9,10] Further research has identified α-solanine (α-Sol) as one of the most important bioactive components of Solanum nigrum. α-Sol is a natural steroidal alkaloid first discovered in 1820 and later widely detected in plants such as potatoes and tomatoes.[10] Although α-Sol is commonly regarded as toxic, its effects on the human body depend on its concentration, and at appropriate doses, it can be beneficial to health. Research has demonstrated that α-Sol possesses a variety of biological activities, including antitumor, antidiabetic, antiallergic, anti-inflammatory, and antiviral effects.[11,12] It has been shown to inhibit the growth of various tumor cells, including liver cancer, lymphoma, colon cancer, gastric cancer, and cervical cancer.[13] Evidence suggests that, in PC, α-Sol can inhibit the proliferation, migration, and invasion of PC cells, thereby suppressing tumor growth.[14] In our previous studies, we further discovered that α-Sol can downregulate the expression of vascular endothelial growth factor (VEGF) in PC by modulating the ERK1/2-HIF-1α and STAT3 signaling pathways, thereby affecting cancer cell proliferation, migration, and invasion.[15] These findings suggest that α-Sol holds promise as an effective drug for the treatment of PC. However, its application remains challenging due to its hydrophobic nature.[16] First, its hydrophobicity, extensive toxicity, and prolonged serum half-life may lead to accumulation in the body following intravenous injection, potentially causing severe adverse effects such as neurological damage and respiratory failure.[12,17] Second, high concentrations of α-Sol can induce strong cytotoxic effects, leading to rapid plasma membrane damage, metabolic disturbances, and ultimately, cell death.[18] Additionally, α-Sol exhibits hemolytic activity, and direct intravenous administration may result in red blood cell lysis, triggering severe side effects such as acute cerebral edema and gastroenteritis.[19] More importantly, the major challenge of intravenous α-Sol administration lies in its poor tumor-targeting ability, resulting in low accumulation in tumor tissues while causing significant systemic toxicity to normal tissues.[20] Therefore, enhancing the tumor-targeting capability of α-Sol while reducing its toxicity remains a critical scientific issue that needs to be urgently addressed.

With the advancement of nanotechnology, various synthetic polymers, such as poly(lactic-co-glycolic acid) and poly-vinylpyrrolidone, have been widely used to minimize side effects and enhance targeted therapy.[21] However, these synthetic nanoparticles (NPs) are prone to being trapped in the reticuloendothelial system, and prolonged use may lead to side effects.[22] Among the various nanocarriers, nature-inspired NPs carriers have attracted considerable attention from researchers.[23] Recently, protein biomolecules have shown potential as ideal drug delivery carriers by overcoming the limitations of traditional therapies, such as poor water solubility, low bioavailability, and ineffective therapeutic outcomes.[24] Among these, serum albumin (SA)-based drug delivery systems have gained popularity due to their selective delivery capabilities, good biodegradability, non-toxicity, safety of metabolic products, ease of purification, excellent water solubility, and lack of immunogenicity. Bovine serum albumin (BSA) is one of the most widely used albumins in biopharmaceutical applications.[25] Studies have shown that BSA NPs, as multifunctional protein carriers for drug delivery, exhibit properties such as non-toxicity, non-immunogenicity, low cost, good biocompatibility, easy metabolism, and excellent water solubility.[26] Additionally, the structure of BSA contains both hydrophobic and hydrophilic domains and is rich in various functional groups, making it suitable for the loading of multiple drugs and functional modifications.[27] Based on the enhanced permeability and retention (EPR) effect and interactions with the Gp60 receptor (a 60 kDa glycoprotein) on endothelial membranes,[28] BSA NPs can accumulate in the tumor microenvironment, increasing the local concentration of drugs within the tumor.[29,30] Several albumin-based drugs or imaging agents have already been launched in the market, and many products are currently in clinical

trials for various applications.[24] Thus, BSA NPs show broad prospects in drug delivery. However, although BSA NPs can increase drug concentration at the tumor site, their tissue penetration remains limited.[28] To overcome these limitations, surface modification of BSA NPs with ligands can enhance their drug targeting, optimize pharmacokinetics and biodistribution, thereby improving therapeutic efficacy and reducing side effects.[28] Polyallylamine hydrochloride (PAH), a polycationic weak base,[31] has been widely used in drug delivery to enhance the stability and delivery efficiency by modifying the surface of polymers and drugs.[32] Research has shown that PAH modification can significantly improve the cellular uptake efficiency of BSA NPs.[32]

Based on this, the aim of this study is to develop a PAH-modified BSA-specific drug delivery system loaded with α-solanine (PAH-BSA-α-Sol NPs, abbreviated as PBSO NPs), to achieve targeted delivery and controlled release, thereby enhancing the therapeutic efficacy of α-solanine, reducing its toxicity, and ultimately achieving the goal of treating pancreatic cancer.

Materials and Methods

Preparation of PAH-BSA-α-Sol NPs (PBSO NPs)

To prepare the BSA solution, 100 mg of BSA was dissolved in 1 mL of double-distilled water (DDW). The resulting BSA solution and 1 mg of $NaBH_4$ were then added to 29 mL of DDW. Subsequently, using a syringe with a 30-gauge needle, 40 mL of 1 mg/mL α-Sol solution was gradually added dropwise into the BSA/$NaBH_4$ mixture under continuous stirring at 1000 rpm for 2 h at 4°C. After the addition was complete, ultrafiltration centrifugation (100 kDa cutoff membrane) was performed for 10 min to remove unreacted $NaBH_4$ and unencapsulated α-Sol. The obtained BSA-α-Sol NPs were then mixed with 30 mg of PAH (5 kDa) and incubated at 4°C for 2 h. Following incubation, another ultrafiltration centrifugation (100 kDa cutoff membrane) was carried out for 10 minutes to remove unreacted PAH, yielding the final PBSO nanoparticles. The resulting nanoparticles were freeze-dried and stored at room temperature in a light-protected environment for further experiments.

Characterization of PBSO NPs

The structure and morphology of the NPs were characterized using transmission electron microscopy (TEM, FEI Talos F200X, USA). The zeta potential and hydrodynamic diameter of the NPs were measured using a nanoparticle size analyzer (Zetasizer Nano ZS, UK). The particle size distribution of the synthesized NPs was determined by dynamic light scattering (DLS), and the chemical modification of the BSA NPs was verified using Fourier transform infrared spectroscopy (FTIR).

In vitro Drug Release

Free α-Sol and PBSO NPs were separately encapsulated in dialysis bags and placed in centrifuge tubes containing 10 mL of PBS. The tubes were maintained at 37°C under gentle stirring to simulate physiological conditions. Sampling time points were set at 0, 1, 2, 4, 6, 8, 12, 18, 24, and 48 h. At each time point, a specific volume of the release medium was withdrawn, filtered through a membrane, and the supernatant was collected. An equal volume of PBS was then added back to maintain a constant total volume of 10 mL. The amount of α-Sol in both free α-Sol and PBSO NPs corresponded to an equivalent dose of 2.6 mg. High-performance liquid chromatography (HPLC, Agilent 1260, USA) was used to determine the α-Sol concentration at different time points to evaluate its release profile.

Cell Culture

Human umbilical vein endothelial cells (HUVECs) and mouse pancreatic cancer cells (Panc02) were obtained from the Chinese Academy of Sciences (Shanghai, China) and Procell Life Science & Technology Co., Ltd. (Wuhan, China), respectively. HUVECs were cultured in DMEM supplemented with 10% fetal bovine serum (FBS) and 1% penicillin/ streptomycin, while Panc02 cells were cultured in RPMI-1640 medium with the same supplements. All cells were maintained in a humidified incubator at 37°C with 5% CO_2. To determine the optimal concentration of PBSO NPs for subsequent experiments, Panc02 cells were exposed to various concentrations of PBSO NPs (0–150 μg/mL) for

24 h. Based on cell viability results, a concentration of 75 μg/mL was selected for further studies. Subsequently, HUVECs and Panc02 cells were divided into four groups: Control, α-Sol, BSA NPs, and PBSO NPs. Except for the Control group, which was cultured in regular medium, the other three groups were treated with media containing α-Sol (2 μg/mL), BSA NPs, or PBSO NPs (75 μg/mL, containing 2 μg/mL of α-Sol) for 24 h. The concentration of α-Sol in α-Sol and PBSO NPs groups was calculated based on the encapsulation efficiency of PBSO NPs.

Cellular Uptake

An in vitro cellular uptake experiment was conducted using Panc02 cells to evaluate the uptake of α-Sol, BSA NPs, and PBSO NPs. To better visualize cellular uptake under different intervention conditions, IR-780 was used to modify α-Sol, BSA NPs, and PBSO NPs. The carboxyl groups on IR-780 were activated to covalently bind with the hydroxyl groups on α-Sol, thereby successfully labeling α-Sol and endowing it with fluorescence properties. Additionally, due to the abundant functional groups of BSA, including carboxyl, amino, and hydrophobic regions, it can interact with IR-780 through multiple mechanisms, such as covalent bonding, electrostatic interactions, and hydrophobic interactions.[33] The specific procedure was as follows: IR-780 was separately incubated with α-Sol, BSA NPs, and PBSO NPs under stirring at room temperature for 24 h, yielding IR780-modified formulations. To ensure consistent fluorescence intensity among IR-780-labeled α-Sol, BSA NPs, and PBSO NPs, fluorescence spectroscopy was used to verify labeling efficiency, and sample concentrations were adjusted accordingly to maintain uniform fluorescence signals across experimental groups before further processing. After labeling, Panc02 cells were seeded in 6-well plates and treated the next day with IR780-labeled α-Sol, BSA NPs, and PBSO NPs. Following a 4h incubation, cells were washed with PBS, fixed with 4% paraformaldehyde (PFA), washed again with PBS, and counterstained with 4′6-diamidino-2-phenylindole (DAPI). Finally, confocal laser scanning microscopy was used to observe cellular uptake.

CCK-8 Assay

Panc02 or HUVEC cells (1 × 10^4 cells per well) were seeded in 96-well plates and divided into different groups according to the experimental design, with at least six replicates per group. When the cell confluence reached approximately 70% under a microscope, the original culture medium was replaced with fresh medium containing different concentrations of PBSO NPs, with or without α-Sol, BSA NPs, or PBSO NPs. The cells were then incubated for an additional 24 h. After discarding the medium, 10 μL of CCK-8 solution was added to each well, and the mixture was incubated for 2 h in the incubator. The absorbance at 450 nm was measured to evaluate cell viability.

Transwell Assay

The Panc02 cells were divided into the Control group, α-Sol group, BSA NPs group, and PBSO NPs group. Except for the Control group, the remaining three groups were incubated with culture medium containing α-Sol (2 μg/mL), BSA NPs, and PBSO NPs (75 μg/mL, with α-Sol at 2 μg/mL) for 24 h. The Control group was incubated with normal culture medium for 24 h. After incubation, cells in the logarithmic growth phase from each group were digested with 0.25% trypsin, and a single-cell suspension was prepared, adjusting the cell concentration to 5×10^5 cells/mL. A 100 μL aliquot of the cell suspension was added to the upper chamber of a Transwell, and 500 μL of culture medium was added to the lower chamber. For the invasion assay, Matrigel matrix gel was pre-coated in the upper chamber. After 36 h, PBS was used to wash the upper chamber, and cells that had passed through the upper chamber were fixed with 4% paraformaldehyde. The cells were stained with 1% crystal violet for 15 min, then inverted and air-dried. Finally, the cells were observed and counted under an inverted microscope, and images were obtained.

Flow Cytometry

Apoptosis of cells was detected using flow cytometry. The Panc02 cells were divided into the Control group, α-Sol group, BSA NPs group, and PBSO NPs group. Except for the Control group, the remaining three groups were incubated with culture medium containing α-Sol (2 μg/mL), BSA NPs, and PBSO NPs (75 μg/mL, with α-Sol at 2 μg/mL) for 24 h. The Control group was incubated with normal culture medium for 24 h. After incubation, cells from each group were collected, and the supernatant was removed by centrifugation. Next, 100 μL of 1× Binding Buffer was added to

resuspend the cells, followed by the addition of 5 μL Annexin V-Alexa Fluor 647 and 10 μL PI. The cells were incubated in the dark at room temperature for 15 min. After incubation, 300 μL of 1× Binding Buffer was added, mixed well, and the samples were placed on ice. Flow cytometry (Beckman Coulter, USA) was used for detection within 1 h.

TUNEL Assay

Apoptosis of cells was detected by TUNEL staining. The TUNEL detection kit (Beyotime) was used according to the manufacturer's instructions to assess apoptosis in Panc02 cells or tumor tissue cells. The treatment method for Panc02 cells was the same as described in section 2.7, while tumor tissue was sourced from section 2.16. Briefly, Panc02 cells and tumor tissue sections were mounted using ProLong anti-fade mounting media with DAPI and observed under a confocal microscope. Images were taken at excitation wavelengths of 488 nm and 405 nm, respectively.

RT-PCR Assay

Total RNA was extracted from treated Panc02 cells or tumor tissue using the Cell/Tissue Total RNA Isolation Kit (Vazyme, Nanjing, China). Subsequently, the RNA was reverse transcribed into cDNA, PCR amplified, with GAPDH serving as an internal reference. The relative expression levels of caspase-3, Bcl-2, and Bax in cells or tissues were calculated using the $2^{-\Delta\Delta CT}$ method for relative quantification. The primer sequences are provided in Table 1.

Western Blot Assay

Total protein samples were extracted from cells or tumor tissue using RIPA lysis buffer. The treatment method for Panc02 cells was the same as described in section 2.7, while the tumor tissue was sourced from section 2.16. Following protein extraction, the protein concentration was determined using the Micro BCA Protein Assay Kit. Equal amounts of protein samples were separated on a 10% sodium dodecyl sulfate-polyacrylamide gel electrophoresis (SDS-PAGE) and transferred to a Polyvinylidene fluoride (PVDF) membrane. The PVDF membrane was blocked with 5% skim milk in TBST at room temperature for 1 h, followed by overnight incubation with primary antibodies (caspase-3: 1:2000; Bcl-2: 1:1000; Bax: 1:2000; β-actin: 1:50,000). After washing three times with Tris-buffered saline, the PVDF membrane was then incubated with secondary antibodies at room temperature for 30 min, followed by detection using a chemiluminescence imaging and analysis system. All antibodies were procured from Proteintech (Wuhan, China).

Animals

All male BALB/c mice used in the experiments were procured from SiPeiFu (Beijing, China). All animal experimental procedures in this study complied with guidelines for the care and use of laboratory animals. The research protocol has been approved by the Animal Care and Ethics Committee of Wenzhou Medical University (Approval No. wydw2024-0551).

In vivo Targeting of PBSO NPs

Panc02 cells (1×10^7 cells/mL, 50 μL) were inoculated into the right flank of BALB/c mice (n=3) to establish a pancreatic cancer xenograft model. When the tumor volume reached approximately 50 mm^3, the mice were intravenously injected with IR-780-modified PBSO NPs (8 mg/kg, containing α-Sol 0.2 mg/kg). Prior to imaging, the experimental mice were anesthetized with 2% isoflurane. At 0, 1, 3, 6, 12, and 24 h post-injection, fluorescence images were obtained using the PerkinElmer IVIS Spectrum. At the end of the experiment, all mice were euthanized under anesthesia with 3% pentobarbital sodium (30 mg/kg). Tumor, heart, liver, spleen, lung, and kidney tissues were then harvested and examined

Table 1 The Primer Sequence

Gene Name	Forward	Reverse
Caspase-3	5′-AGGGGTCATTTATGGGACA-3′	5′-TACACGGGATCTGTTTCTTTG-3′
Bcl-2	5′-GTCATGTGTGTGGAGAGCGTC-3′	5′-CCGTACAGTTCCACAAAGGCATC-3′
Bax	5′-GCTGACATGTTTGCTGATGG-3′	5′-GATCAGCTCGGGCACTTTAG-3′
GAPDH	5′-TCACCACCATGGAGAAGGC-3′	5′-GCTAAGCAGTTGGTGGTGCA-3′

under the same conditions for ex vivo fluorescence imaging analysis, with fluorescence intensity quantified using the IVIS spectrum method.

In vivo Biodistribution of PBSO NPs

The method for constructing the pancreatic cancer xenograft mouse model is the same as described in section 2.14 (ie, using Panc02 cells to establish the pancreatic cancer xenograft tumor model). When the tumor size reached approximately 50 mm^3, 24 BALB/c mice were randomly divided into two groups: α-Sol group and PBSO NPs group, with 12 mice in each group. Mice in the respective groups were intravenously injected with α-Sol (0.2 mg/kg) or PBSO NPs (8 mg/kg, containing 0.2 mg/kg of α-Sol). At designated time points (0.5 h, 1 h, 3 h, and 6 h), three mice from each group were randomly selected and euthanized under anesthesia with 3% pentobarbital sodium (30 mg/kg). Major organs (heart, liver, spleen, lung, and kidney) and tumor tissues were harvested, and the drug content in each tissue was determined using HPLC.

In vivo Anti-Tumor Activity of PBSO NPs

The construction method of the pancreatic cancer xenograft mouse model for in vivo targeting is as follows. After the tumors naturally grew and formed for 7 days, 20 BALB/c mice were randomly divided into four groups: Control group, α-Sol group, BSA NPs group, and PBSO NPs group, with 5 mice in each group. Mice in the respective groups were intravenously injected with saline (Control), α-Sol (0.2 mg/kg), BSA NPs, or PBSO NPs (8 mg/kg, containing 0.2 mg/kg of α-Sol) for intervention treatment, with injections given every 2 days. Tumor size was measured every 3 days during the experiment. Tumor volume was calculated using the formula: V (mm^3) = 0.5 × tumor maximum diameter × tumor perpendicular diameter^2. After 30 days of Panc02 cell injection, all mice in each group were euthanized under anesthesia with 3% pentobarbital sodium (30 mg/kg), followed by photography, tumor tissue collection, and weighing for further experiments.

Pathological Examination

The pathological changes in mouse tumor tissues were evaluated using the hematoxylin and eosin (H&E) staining method. Tissues were fixed in 4% paraformaldehyde, dehydrated, embedded, sectioned into 5 μm paraffin slices, and stained with H&E. Following washing, mounting, and drying, the tumor tissue pathological alterations were observed under a microscope.

Hemolysis Assay in vitro

Using red blood cells isolated from healthy mouse blood for hemolysis assessment. In brief, red blood cells (RBCs) were collected by centrifuging fresh blood samples from healthy mice to remove serum (5000 rpm, 5 min). The RBCs were washed, resuspended, and diluted with PBS to achieve a final concentration of 16% (v:v). Subsequently, 0.5 mL of diluted RBCs were mixed with 0.5 mL of PBSO NPs at different concentrations (20, 50, 100, 200 μg/mL). Deionized water served as the positive control, and PBS solution as the negative control. All test samples were then incubated at 37°C for 1 h, followed by centrifugation at 3000 rpm for 10 min, and the supernatant was collected to measure the absorbance at 540 nm. The hemolysis percentage was calculated using the formula:

$$\text{Hemolysis}(\%) = \frac{\text{OD}_{\text{sample}} - \text{OD}_{\text{negative}}}{\text{OD}_{\text{positive}} - \text{OD}_{\text{negative}}} \times 100\%.$$

Serum Biochemical Analysis

Twenty BALB/c mice provided by SiPeiFu company (Beijing, China) were randomly divided into the Control group, 5d group, 10d group, and 15d group, with 5 mice in each group. The mice in the four groups were injected via the tail vein with either PBS or PBSO NPs (8 mg/kg, containing 0.2 mg/kg of α-Sol). Twelve hours later, all mice were euthanized under anesthesia with 3% pentobarbital sodium (30 mg/kg).After euthanizing all mice, blood samples were collected from each group. Serum levels of alanine aminotransferase (ALT), aspartate aminotransferase (AST), creatinine (CRE), and blood urea nitrogen (BUN) were measured using an automated chemistry analyzer, following the method described previously.[34]

HE Staining

Nine healthy BALB/c nude mice provided by SiPeiFu company (Beijing, China) were randomly divided into the Control group, α-Sol group, and PBSO NPs group, with 3 mice in each group. Mice in the three groups were intravenously injected with PBS, α-Sol (0.2 mg/kg), and PBSO NPs (8 mg/kg, containing 0.2 mg/kg of α-Sol), respectively. After 24 h of treatment, all mice were euthanized, and heart, lung, liver, spleen, and kidney tissue samples were collected. HE staining method was used to evaluate the histopathology of heart, lung, liver, spleen, and kidney tissue sections from mice in the Control, α-Sol, and PBSO NPs groups.

Statistical Analyses

All experiments were repeated at least three times. All data are presented as mean ± standard deviation. Statistical analysis was performed using GraphPad Prism 9 software (GraphPad Inc, San Diego, CA, USA). Student's *t*-test was used for comparisons between two groups, while one-way analysis of variance (ANOVA) was used for comparisons among multiple groups. A *P*-value of less than 0.05 was considered statistically significant.

Results

Characterization of PBSO NPs

To address the challenges of α-Sol in clinical applications, we designed and synthesized a nanoparticle delivery system (PBSO NPs) based on PAH-modified BSA loaded with α-Sol. In this study, we used a green method based on $NaBH_4$ reduction-induced denaturation and drug-induced self-assembly to prepare BSA NPs.[35] Under the action of the reducing agent $NaBH_4$, some of the disulfide bonds in BSA were reduced, leading to a relaxation of the protein conformation and exposing its hydrophobic core regions. Hydrophobic drug α-Sol was then added, interacting with the hydrophobic regions of BSA and inducing BSA self-assembly, forming BSA-α-Sol nanoparticles (BSA-α-Sol NPs). Subsequently, by introducing the positively charged PAH, which can bind to the negatively charged BSA NPs through electrostatic interactions, the stability of the nanoparticles was further improved, thus forming PBSO NPs. The morphological structures of BSA NPs and PBSO NPs were examined using TEM. The results (Figure 1A) showed that both BSA NPs and PBSO NPs appeared as irregularly sized spherical nanoparticles, indicating that α-Sol loading and PAH surface modification did not affect their morphology. The FTIR results (Figure 1B) of PBSO NPs showed N-H stretching vibration peaks at 3500 cm^{-1}, 3432 cm^{-1}, and 3044 cm^{-1}, confirming the successful PAH modification. Studies have shown that the optimal size of drug carriers is 100–200 nm. This small size facilitates the effective delivery of the drug to the targeted tumor site.[36] Therefore, we utilized a nanoparticle size analyzer to measure the particle size of BSA NPs and PBSO NPs. The results (Figure 1C) showed that the particle size of BSA NPs was 82.87 ± 3.81 nm, which increased to 90.70 ± 1.24 nm after loading α-Sol and modification with PAH, falling within the ideal size range for tumor therapy. Further zeta potential analysis (Figure 1D) indicated that BSA NPs carried a negative surface charge[37] with a zeta potential of approximately −21.73 mV. After modification with positively charged PAH and loading α-Sol, the overall charge of PBSO NPs became positive, with a zeta potential of approximately 31.47 mV, confirming the successful modification of PAH on the surface of BSA NPs. The stability of drug delivery carriers in the medium is crucial.[38,39] Therefore, we evaluated the stability of BSA NPs and PBSO NPs in deionized water. The results (Figure 1E) demonstrated that both NPs maintained a stable size distribution after dispersing in water for seven days, suggesting that PBSO NPs have potential advantages in drug delivery. Moreover, in vitro drug release analysis (Figure 1F) revealed that free α-Sol exhibited a burst release in simulated body fluid, with almost no detectable drug remaining after 24 h. In contrast, PBSO NPs released only 60% of α-Sol within 48 h and continued to release the drug over time, indicating that PBSO NPs effectively mitigate the burst release effect and enable sustained drug release.

Cellular Uptake of PBSO NPs

Any nanocarrier must traverse the cell membrane barrier to enter the intracellular environment, where it releases the delivered therapeutic drug to exert its therapeutic effects. Therefore, cellular uptake of nanoparticles is a critical initial step for successful drug delivery.[40] To investigate the cellular uptake of PBSO NPs, this study utilized IR-780 to label α-Sol, BSA NPs, and PBSO NPs, and the intracellular fluorescence intensity of IR-780 was measured to evaluate cellular
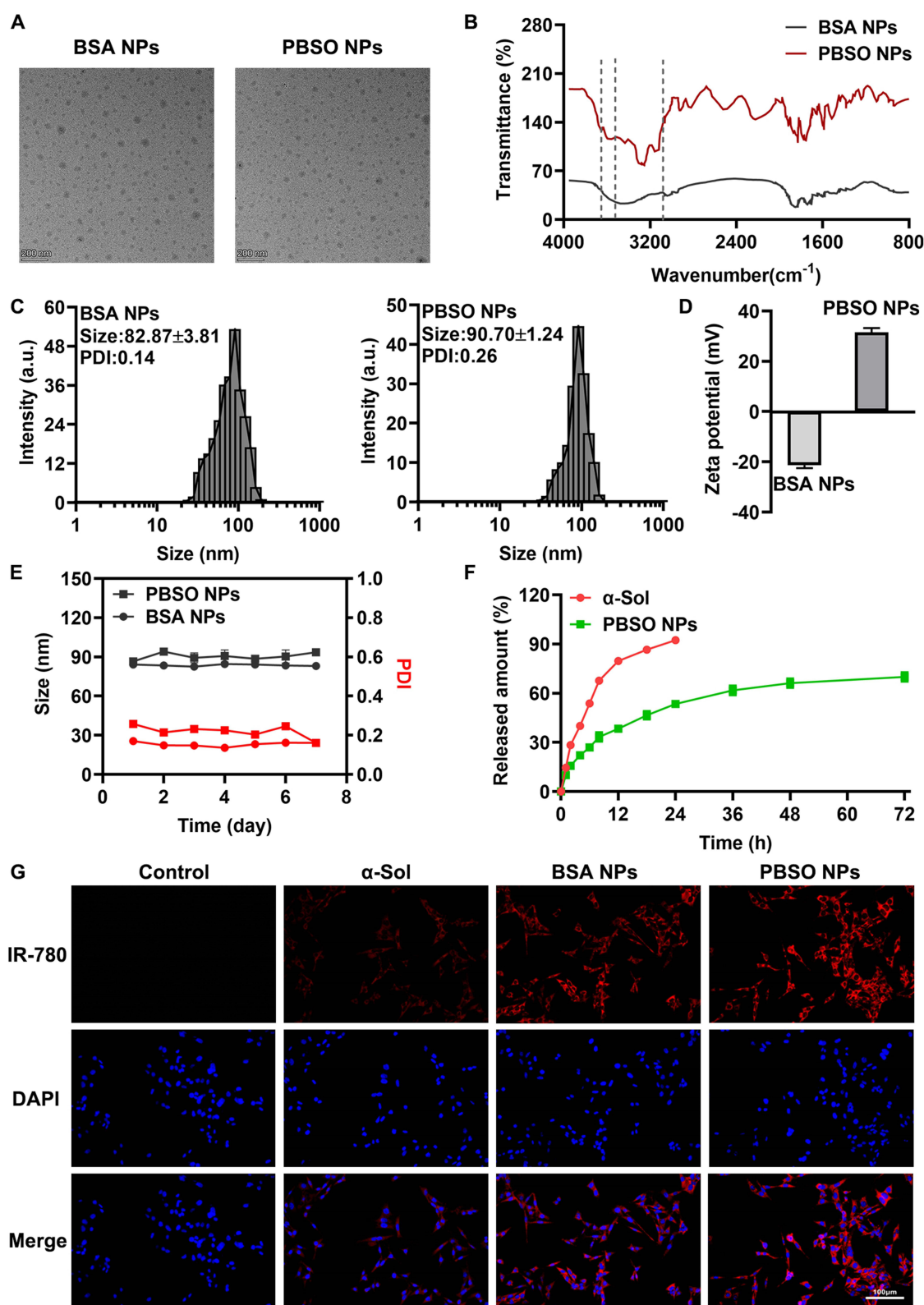
Figure 1 Characterization of PBSO NPs. (**A**) TEM images of BSA NPs and PBSO NPs, scale bar = 200 nm. (**B**) FTIR analysis of BSA NPs and PBSO NPs. (**C**) Particle size of BSA NPs and PBSO NPs. (**D**) Zeta potential of BSA NPs and PBSO NPs. (**E**) Stability of BSA NPs and PBSO NPs. (**F**) In vitro drug release profiles of free α-Sol and PBSO NPs. G, Cellular uptake of PBSO NPs in Panc02 cells, Bar = 100 nm.

uptake of the nanocarriers. The results (Figure 1G) showed that, compared to the Control group, distinct IR-780 fluorescence signals were observed in Panc02 cells treated with α-Sol, BSA NPs, and PBSO NPs. Among them, the BSA NPs group exhibited stronger fluorescence signals than the α-Sol group, while the PBSO NPs group displayed the highest fluorescence intensity, which was significantly higher than that of the BSA NPs group. These findings indicate that PBSO NPs significantly enhance cellular uptake efficiency.

In vitro Anti-PC Activity of PBSO NPs

We successfully synthesized PBSO NPs for the delivery of α-Sol and further evaluated their in vitro effects on Panc02 cells. First, after treating Panc02 cells with different concentrations of PBSO NPs for 24 h the cell viability was assessed using the CCK-8 assay. As shown in Figure 2A, Panc02 cell viability exhibited a dose-dependent decrease with increasing concentrations of PBSO NPs (0–150 μg/mL), with an IC50 value of approximately 75 μg/mL. Therefore, 75 μg/mL was selected as the concentration for subsequent experiments. To further investigate the effects of α-Sol and PBSO NPs on PC cells, Panc02 cells were cultured in vitro and subjected to different treatments to evaluate their impact on cell viability, migration, invasion, and apoptosis. The CCK-8 assay results (Figure 2B and C) showed that, compared to the Control group, both α-Sol and PBSO NPs significantly reduced cell viability ($P<0.001$), with no significant effects on HUVEC viability. Additionally, the CCK-8 results indicated that PBSO NPs exhibited a more pronounced inhibitory effect on Panc02 cell viability than free α-Sol, demonstrating a stronger anti-tumor effect without cytotoxicity. The Transwell assay results (Figure 2D–F) revealed that, compared to the Control group, both α-Sol and PBSO NPs significantly inhibited Panc02 cell migration and invasion ($P<0.05$), with PBSO NPs exhibiting a more pronounced inhibitory effect. Furthermore, flow cytometry analysis (Figure 2G and H) demonstrated that both α-Sol and PBSO NPs significantly induced apoptosis in Panc02 cells, with PBSO NPs exhibiting a stronger pro-apoptotic effect. Multiple studies have reported that apoptosis induction is one of the primary mechanisms by which α-Sol exerts its anti-tumor effects.[41–43] To further explore the impact of PBSO NPs on apoptosis in PC cells, we conducted TUNEL assay, RT-PCR, and Western blot assays to analyze the expression levels of apoptosis-related proteins (caspase-3, Bcl-2, and Bax) in Panc02 cells. The TUNEL assay results (Figure 3A) showed a significant increase in fluorescence intensity and the number of TUNEL-positive cells in the α-Sol and PBSO NPs groups compared to the Control group. Moreover, RT-PCR and Western blot results (Figure 3B and C) demonstrated that, compared to the Control group, caspase-3 and Bax expression levels were significantly upregulated ($P<0.05$), while Bcl-2 expression was significantly downregulated ($P<0.05$) in the α-Sol and PBSO NPs groups. In conclusion, these findings indicate that both α-Sol and PBSO NPs effectively inhibit PC cell growth by suppressing cell viability, migration, and invasion while promoting apoptosis.

In vivo Biodistribution of PBSO NPs

To evaluate the in vivo biodistribution of PBSO NPs, PBSO NPs were intravenously injected into pancreatic cancer xenograft mice for in vivo imaging analysis. Fluorescence imaging results (Figure 4A) revealed that, 4 h after the injection of PBSO NPs, fluorescence began to gradually accumulate at the tumor site and remained stably localized there. Strong fluorescence was still detectable at the tumor site 24 h post-injection, indicating that PBSO NPs effectively delivered α-Sol to the tumor tissue. Further ex vivo fluorescence imaging of the tumor and major organs (Figure 4B) showed the strongest fluorescence in the tumor tissue. This is likely related to the endocytosis of cancer cells and the involvement of Gp60 receptors. Generally, due to the nanoparticle size effect, cancer cells can effectively internalize NPs via endocytosis. Moreover, Gp60 is highly expressed in the endothelial cells surrounding tumors, and the BSA carrier can effectively bind to Gp60 to form a BSA-Gp60 complex in caveolae. This complex can cross the tumor stroma via Gp60-mediated transcytosis, thereby enhancing the fluorescence intensity in tumor tissues.[44,45] Additionally, we assessed the distribution of free α-Sol and PBSO NPs in various organs and tissues after injection. The results (Figure 4C and D) showed that free α-Sol primarily distributed in the liver and kidneys, and was also widely distributed in the heart, spleen, lungs, and tumor tissues. In contrast, the distribution of PBSO NPs in tumor tissues was significantly increased, while their distribution in the heart, liver, spleen, lungs, and kidneys was reduced. This suggests that PBSO NPs can reduce the distribution of the drug to other organs, thereby alleviating drug toxicity. Overall, PBSO NPs demonstrated good performance in delivering α-Sol specifically to tumor sites.
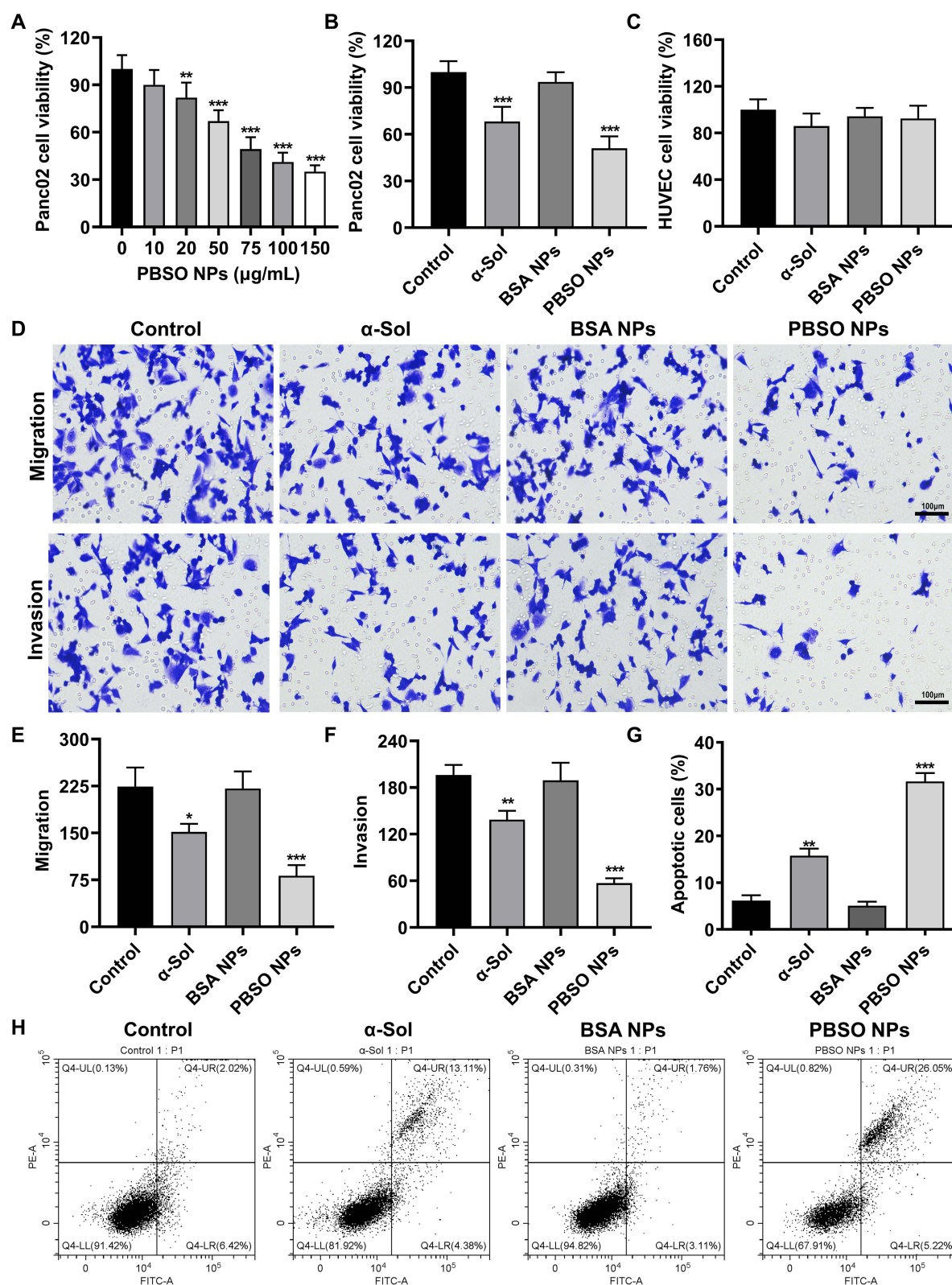
Figure 2 PBSO NPs inhibit Panc02 cell viability, invasion, and migration while promoting apoptosis. (**A**) Effects of different concentrations of PBSO NPs on Panc02 cell viability. (**B**) Effects of PBSO NPs on cell viability. (**C**) Effects of PBSO NPs on the viability of HUVECs. (**D**–**F**), Transwell assay results showing the effects of PBSO NPs on cell invasion and migration. (**G**–**H**), Flow cytometry analysis of the effects of PBSO NPs on cell apoptosis. *$P<0.05$ vs Control or 0 μg/mL, **$P<0.01$ vs Control or 0 μg/mL, ***$P<0.001$ vs Control or 0 μg/mL.

A

B

C
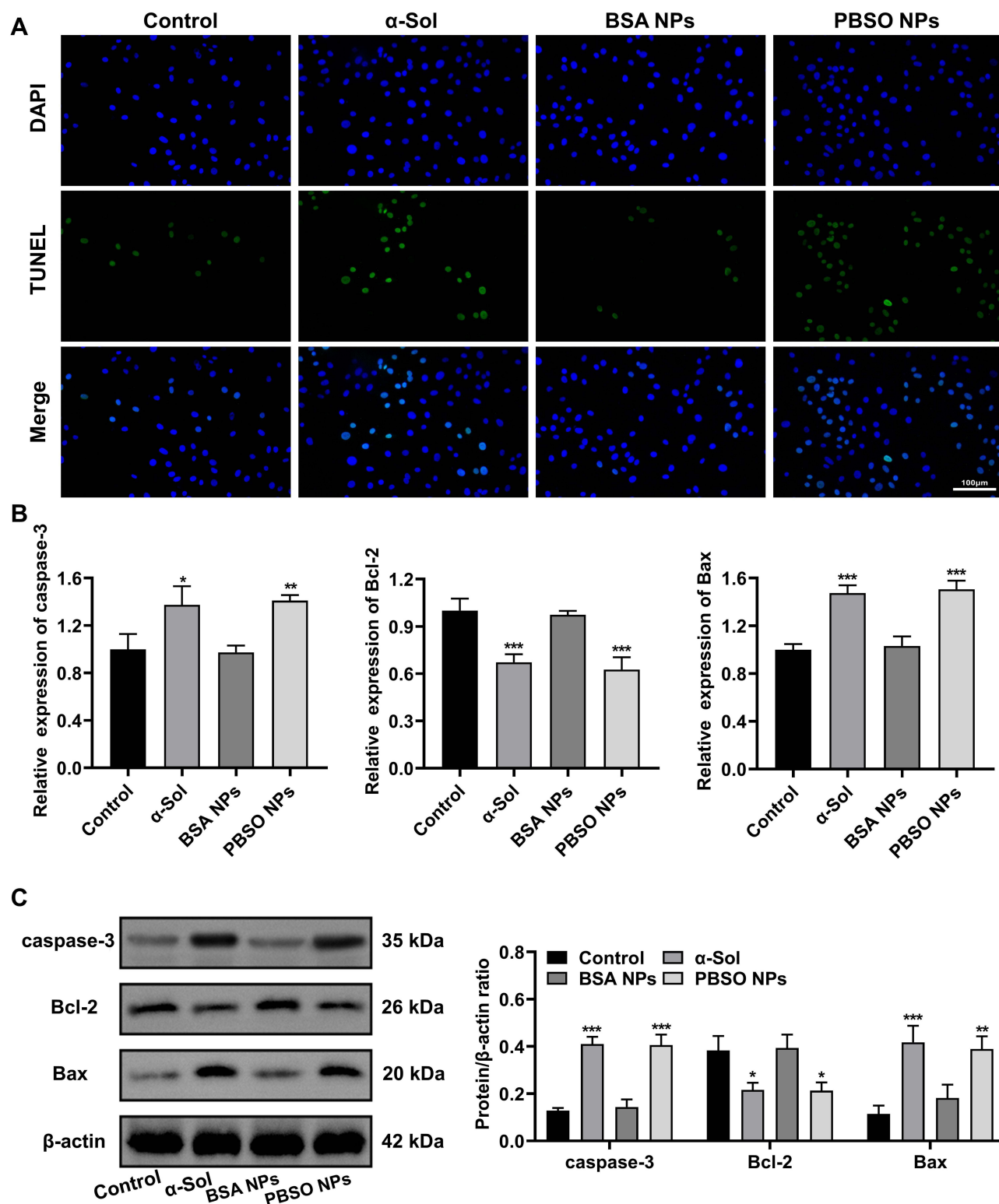
Figure 3 PBSO NPs promote apoptosis in Panc02 cells. (**A**) TUNEL assay for detecting cell apoptosis. (**B**) RT-PCR analysis of caspase-3, Bcl-2, and Bax expression levels in cells. (**C**) Western blot assay for caspase-3, Bcl-2, and Bax expression levels in cells. $*P<0.05$ vs Control, $**P<0.01$ vs Control, $***P<0.001$ vs Control.
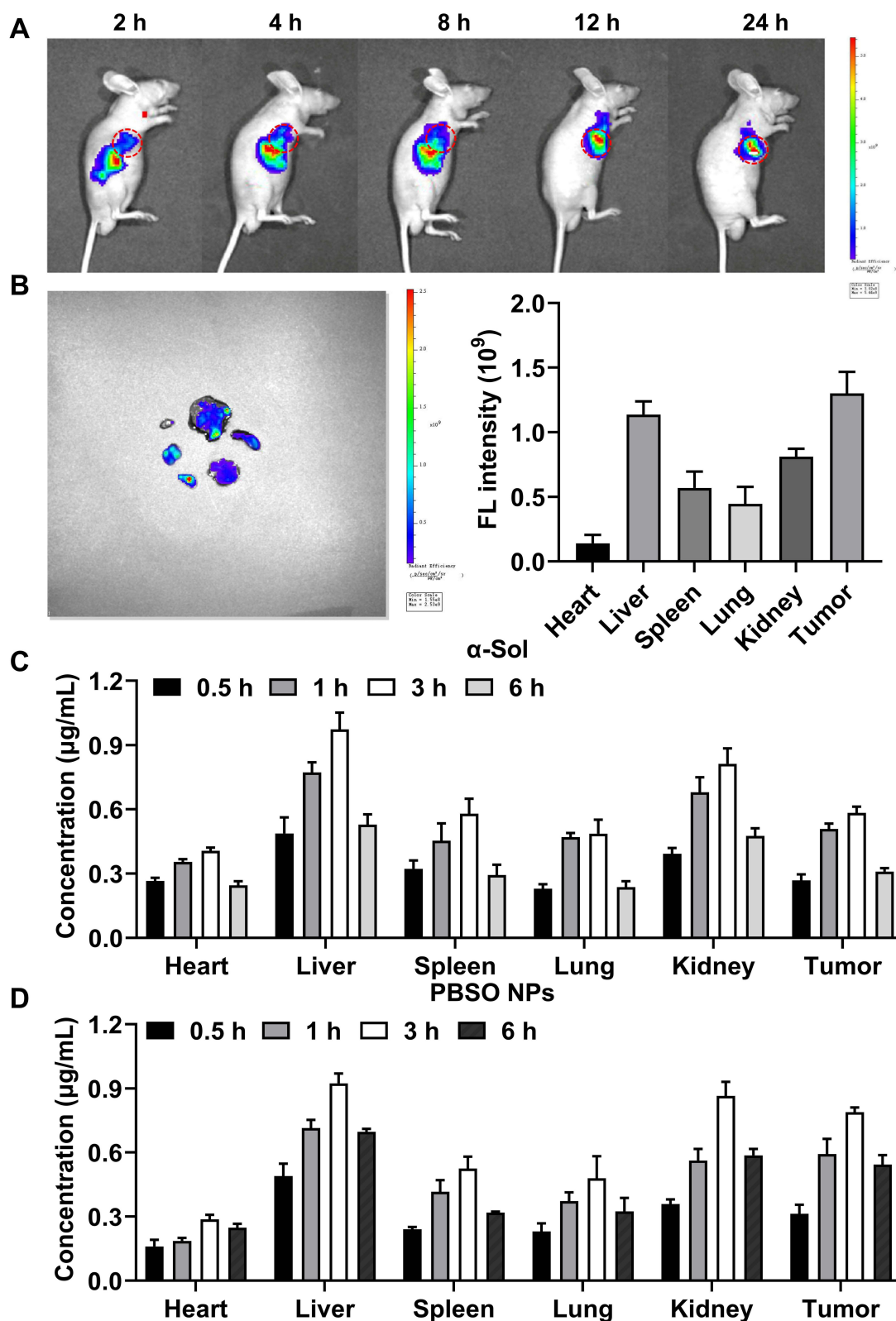
Figure 4 PBSO NPs exhibit good tumor targeting and biodistribution. (**A**) In vivo fluorescence imaging (n=3). (**B**) Ex vivo fluorescence imaging of tumor tissue and major organs (n=3). (**C** and **D**), Distribution of α-Sol and PBSO NPs in major organs and tumor tissue (n=3).

In vivo Antitumor Activity of PBSO NPs

Based on previous experimental studies, we have demonstrated that PBSO NPs can inhibit the growth of PC cells in vitro. To further investigate the in vivo antitumor activity of PBSO NPs, we established a PC xenograft mouse model and applied different treatment interventions. The results (Figure 5A–D) showed that, compared to the Control group, tumor volume and weight were significantly reduced in the α-Sol and PBSO NPs groups ($P<0.05$), with PBSO NPs exhibiting a more significant inhibitory effect on tumor volume and weight, indicating that PBSO NPs enhance the antitumor effects of α-Sol. Further H&E staining results revealed that in the Control and BSA NPs groups, tumor cells were closely packed with intact cell morphology and clear cell nuclei, while in the α-Sol group, localized necrosis was observed in tumor tissue, and in the PBSO NPs group, extensive necrosis was present with loose cell arrangement and cell rupture (Figure 5E), suggesting that both α-Sol and PBSO NPs effectively inhibit tumor growth. Additionally, TUNEL staining, RT-PCR, and Western blot analysis (Figure 6) confirmed that both α-Sol and PBSO NPs promote cell apoptosis, significantly increasing the expression of caspase-3 and Bax in tumor tissues ($P<0.01$) while inhibiting the expression of Bcl-2 ($P<0.01$), consistent with the apoptotic effects observed in vitro. These results indicate that PBSO NPs not only enhance the antitumor effects of α-Sol but also inhibit the progression of PC by promoting cell apoptosis.

Biological Safety Evaluation of PBSO NPs

In vivo biological safety evaluation is a critical factor in assessing the clinical feasibility of nanoparticle-based drugs.[46] Therefore, we conducted an in-depth study on the biological safety of PBSO NPs. Currently, most nanomaterials are administered intravenously. Upon entering the bloodstream, these nanomaterials first interact with various biomolecules in the body fluids. Red blood cells account for 40%-50% of the total blood volume, making them a common subject of study for evaluating the blood compatibility of nanomaterials. Hemolysis rate is the most fundamental indicator of blood compatibility. When nanomaterials come into contact with red blood cells, their hydrophobic interactions and irregular shapes may disrupt the cell membrane, leading to hemoglobin release and causing hemolysis.[47] Therefore, studying hemolysis is a key safety factor in avoiding severe side effects during in vivo drug administration.[48] The hemolysis assay results in this study (Figure 7E) showed that even at a PBSO NPs concentration of 200 μg/mL, the hemolysis rate remained below 5%. This indicates that PBSO NPs are non-hemolytic and can serve as a blood-compatible system for drug delivery applications. Further serum chemistry analysis (Figure 7A–D) indicated that the levels of ALT, AST, BUN, and CRE in all groups were within the normal range, demonstrating that PBSO NPs treatment did not affect liver and kidney function. Moreover, 24 h after drug administration, we performed HE staining on the heart, liver, spleen, lung, and kidney tissues of the mice. The HE staining results (Figure 7F) showed that, except for the α-Sol group, no significant pathological lesions or inflammation were observed in the organs of the Control and PBSO NPs groups. However, mild inflammatory cell infiltration was observed in the heart tissue of the α-Sol group, suggesting potential cardiac toxicity. These findings indicate that PBSO NPs did not cause organ damage in the mice and could reduce the toxicity of free α-Sol. In conclusion, these results demonstrate that PBSO NPs are nanoparticles with good biological safety and hold potential for clinical applications.

Discussion

α-Sol is a steroidal glycoalkaloid derived from potatoes and has been shown to inhibit the proliferation, migration, and invasion of PC cells, thereby preventing PC progression.[14] However, the in vivo tumor-targeting ability of α-Sol is relatively poor, leading to low accumulation in tumor tissues and high systemic toxicity to normal tissues.[20] These adverse effects severely limit the clinical application of α-Sol. Additionally, the hydrophobic nature of α-Sol may further hinder its therapeutic efficacy.[16] Therefore, improving the targeting ability of α-Sol and reducing its side effects to enhance its therapeutic effect on PC has become an urgent issue to address. To this end, this study designed and synthesized a novel PAH-modified BSA nanoparticle (PBSO NPs) for α-Sol delivery. These nanoparticles exhibit favorable morphology and physiological stability, enhance cellular uptake, and effectively improve the anti-PC activity of α-Sol. The findings of this study suggest that PBSO NPs represent a promising drug delivery system for α-Sol, providing new strategies and approaches for PC treatment.

 4247
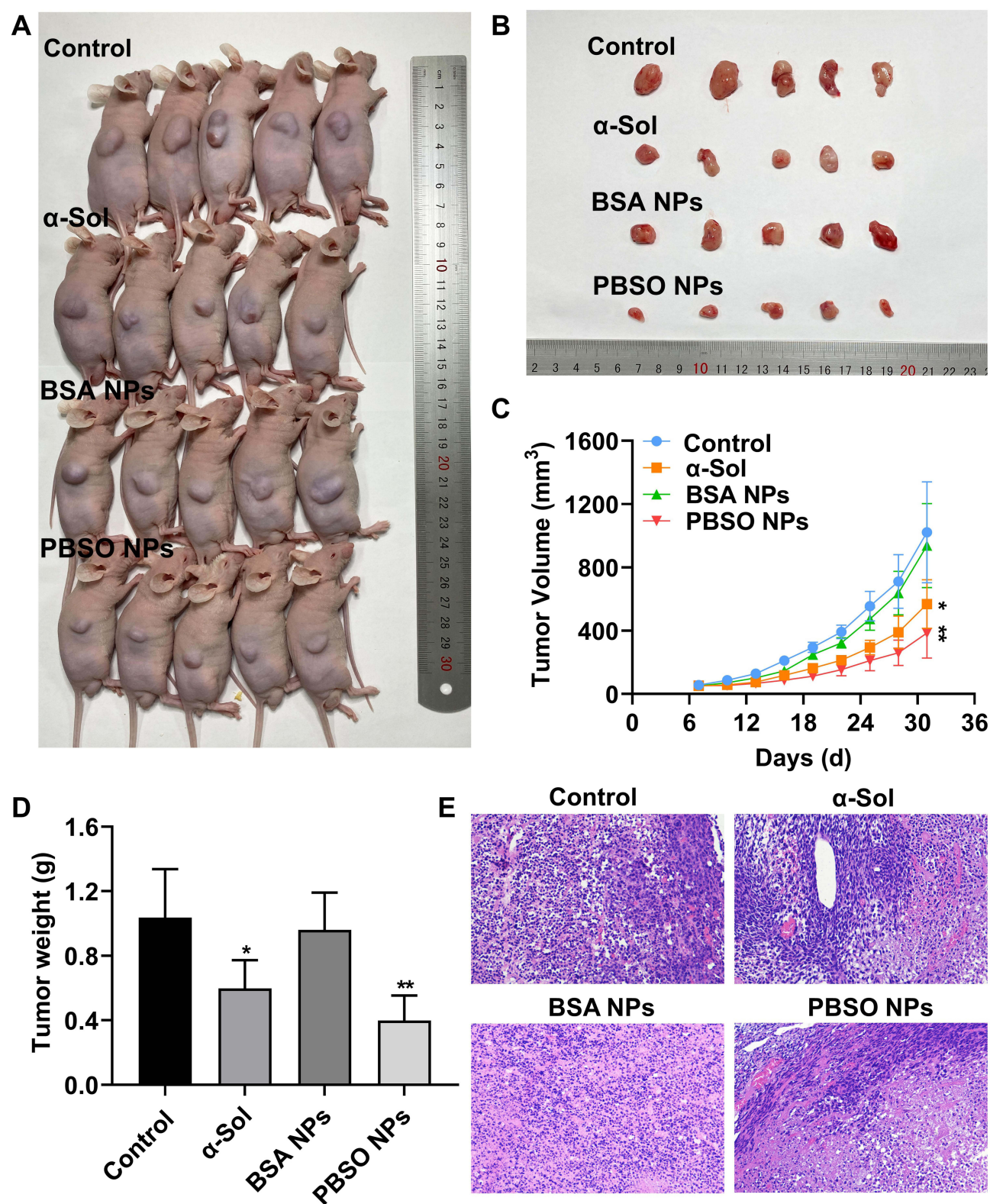
Figure 5 In vivo antitumor activity of PBSO NPs in PC. (**A**) Images of mice from each group (n=5). (**B**) Tumor tissue images from each group (n=5). (**C**) Changes in tumor volume of mice in each group (n=5). (**D**) Changes in tumor weight of mice in each group (n=5). (**E**) H&E staining images of tumor tissue from each group (n=5). *$P<0.05$ vs Control, **$P<0.01$ vs Control. Control, PC xenograft mice injected with physiological saline via tail vein. α-Sol, PC xenograft mice treated with α-Sol via tail vein injection. BSA NPs, PC xenograft mice treated with BSA NPs via tail vein injection. PBSO NPs, PC xenograft mice treated with PBSO NPs via tail vein injection.
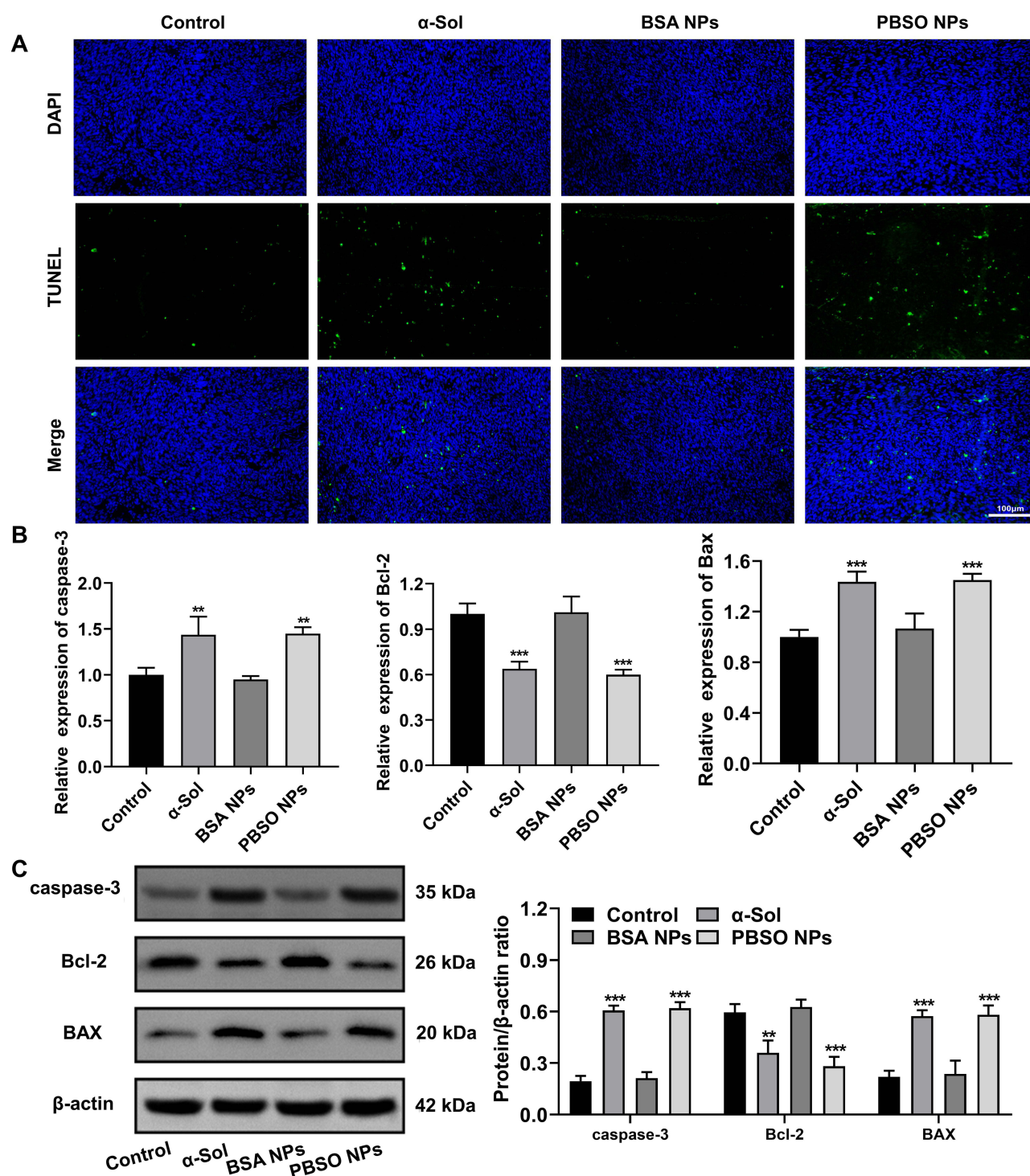
Figure 6 PBSO NPs promote cell apoptosis. (**A**) TUNEL staining to detect cell apoptosis (n=3). (**B**), RT-PCR to detect the expression levels of caspase-3, Bcl-2, and Bax (n=3). (**C**) Western blot assay to detect the expression levels of caspase-3, Bcl-2, and Bax (n=3). **$P<0.01$ vs Control, ***$P<0.001$ vs Control.

Encapsulating drugs within nanocarriers for in vivo delivery has been proven to be an effective strategy for enhancing drug stability and tissue penetration while reducing adverse effects[49] Currently, the US Food and Drug Administration has approved more than 900 nanotechnology-based anticancer drugs for clinical trials, yet only a few have successfully reached the market.[50] Although some nanomedicines can mitigate toxicity to a certain extent, they still fail to completely eliminate adverse effects. As a result, the currently developed nanomedicines have yet to meet the expectations for highly
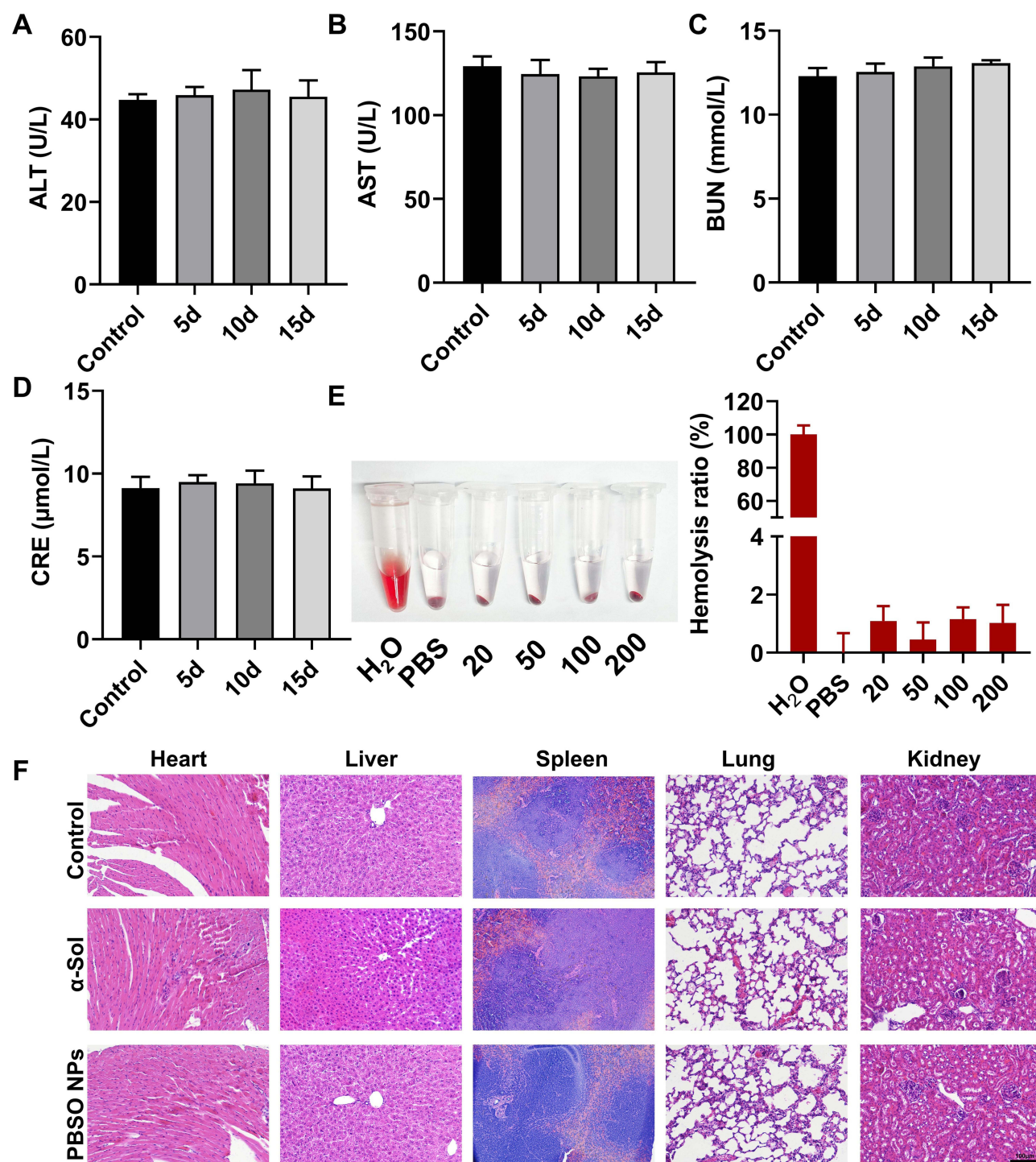
Figure 7 PBSO NPs exhibit good biocompatibility. (**A**–**D**), Detection of ALT, AST, BUN, and CRE levels in serum using an automatic biochemical analyzer (n=5). (**E**) Blood compatibility test. (**F**), HE staining to detect pathological changes in the heart, liver, spleen, lung, and kidney of mice (n=3). ALT, alanine aminotransferase. AST, aspartate aminotransferase. BUN, blood urea nitrogen. CRE, creatinine. Control group, BALB/c nude mice treated with PBS via tail vein injection. 5d, BALB/c nude mice treated with PBSO NPs via tail vein injection for 5 days. 10d, BALB/c nude mice treated with PBSO NPs via tail vein injection for 10 days. 15d, BALB/c nude mice via tail vein injection for 15 days. α-Sol, BALB/c nude mice treated with α-Sol via tail vein injection. PBSO NPs, BALB/c nude mice treated with PBSO NPs via tail vein injection.

efficient, safe, and low-toxicity cancer treatments.[51,52] BSA NPs have been widely utilized for loading hydrophobic drugs to enhance their solubility due to their amphiphilic nature and the abundance of functional groups within their primary structure.[53,54] Additionally, BSA NPs can enhance drug accumulation in tumor tissues by promoting the enhanced permeability and retention (EPR) effect and interacting with proteins such as SPARC.[28] On the other hand, PAH modification of nanoparticle surfaces has been shown to improve their stability and delivery efficiency. Previous studies have demonstrated that PAH-modified BSA NPs significantly enhance cellular uptake.[32] Therefore, this study developed a novel PAH-modified BSA nanocarrier (PBSO NPs) to synergistically enhance the targeted delivery of α-Sol, thereby improving its therapeutic efficacy against PC. It is well established that nanoparticle size significantly influences their biodistribution.[55] Nanoparticles with a size range of 10–100 nm and moderate positive charge are more favorable for tumor-targeted delivery, whereas those smaller than 10 nm are rapidly cleared by the kidneys, and those larger than 100 nm face challenges in penetrating tumor vasculature.[56] The PBSO NPs synthesized in this study exhibited an average particle size of 90.70 ± 1.24 nm, aligning with the optimal range for tumor targeting and meeting the requirements for intravenous administration.[57] Furthermore, while BSA NPs naturally exhibit a negative surface charge,[58] PAH, a weakly basic polycation, effectively modified the surface of PBSO NPs, resulting in a positively charged nanoparticle. This finding is consistent with the study conducted by Choi, J. S. et al.[32] These results suggest that the particle size and surface charge properties of PBSO NPs contribute to improving the tumor-targeted delivery efficiency of α-Sol. Further stability assessments and in vitro drug release experiments demonstrated that PBSO NPs exhibit excellent stability and sustained release properties. This stability may be attributed to the inherent storage stability of BSA,[59] whereas the sustained release effect could be associated with surface charge alterations following PAH modification. As a polycation, PAH likely interacts electrostatically with the negatively charged surface of BSA, reinforcing the structural stability of the nanoparticles and restricting the rapid release of α-Sol to achieve a sustained release effect.[32]

Efficient cellular uptake of drugs is critical for their therapeutic efficacy.[60] In this study, we found that BSA NPs exhibited a higher cellular uptake rate compared to free α-Sol. This may be attributed to the ability of BSA NPs to interact with specific receptors overexpressed on tumor cell surfaces, particularly the secreted protein acidic and rich in cysteine (SPARC), thereby facilitating endocytosis. SPARC, also known as osteonectin, is a matricellular glycoprotein[61] that can be directly expressed and secreted by tumor cells.[62] It is highly expressed in various cancers, including breast cancer, lung cancer, PC, and melanoma,[61] while its expression in normal tissues is relatively low.[62] In PC, SPARC has been identified as a potential therapeutic target due to its involvement in cell proliferation, migration, metastasis, and immune evasion mechanisms.[63] Studies have shown that SPARC serves as a natural ligand for albumin,[62] demonstrating a high binding affinity for albumin.[64] Its overexpression promotes the cellular internalization of albumin-based nanoparticles[65] and has been proven to enhance the penetration and uptake of albumin nanomedicines in tumors.[66] Additionally, research by Lu et al[67] demonstrated that BSA NPs could increase drug cellular uptake. Consistent with these findings, our study also confirmed that BSA NPs enhanced the uptake of α-Sol in PC cells. Further analysis revealed that compared to the BSA NPs group, the PBSO NPs group exhibited significantly stronger IR-780 fluorescence signals in Panc02 cells, indicating that PAH modification further enhanced the cellular uptake efficiency of BSA NPs. Previous studies have demonstrated that cell membranes are negatively charged, and nanoparticles (NPs) with a positively charged surface exhibit faster and higher internalization rates, thereby facilitating cellular uptake and intracellular transport.[68] In contrast, negatively charged NPs tend to have higher absorption rate constants, resulting in slower and lower cellular internalization efficiency.[32,69–71] In this study, the PAH modification of BSA NPs conferred an overall positive charge to PBSO NPs, leading to significantly higher cellular uptake efficiency compared to negatively charged BSA NPs. Furthermore, PBSO NPs demonstrated excellent biocompatibility, with a hemolysis rate below 5%, meeting the standards set by the American Society for Testing and Materials (ASTM), which considers hemolysis rates below 5% indicative of good blood compatibility.[72] Serum biochemical analysis and hematoxylin-eosin (HE) staining results further confirmed that PBSO NPs did not cause damage to liver and kidney functions or major organs. Additionally, compared to free α-Sol, PBSO NPs were able to mitigate the toxicity of α-Sol to a certain extent.

Previous studies have demonstrated that α-Sol exerts antitumor effects by inducing apoptosis and inhibiting the proliferation, migration, and invasion of various cancer cells, including PC cells.[14,43] Among these mechanisms, apoptosis is a fundamental biological process in multicellular organisms, playing a crucial role in eliminating abnormal or unnecessary cells. This process is

not only essential for biological evolution, homeostasis maintenance, and the development of various systems,[73] but it is also recognized as a key defense mechanism by which the host combats tumor cells.[43] As a result, apoptosis induction has become a major focus in cancer therapy research.[10] Multiple studies have shown that apoptosis induction is one of the core mechanisms underlying the antitumor effects of α-Sol.[42,43] Consistent with previous findings, our in vitro and in vivo experiments further confirmed that α-Sol effectively inhibits PC cell proliferation, migration, and invasion while inducing apoptosis. Moreover, PBSO NPs were found to enhance the antitumor activity of α-Sol against PC. Additionally, our in vivo results revealed that PBSO NPs increased the accumulation of α-Sol in tumor tissues while reducing its distribution in other organs, indicating that PBSO NPs improved the selective delivery efficiency of α-Sol. Studies have shown that BSA NPs can bind to Gp60 to form a BSA-Gp60 complex, which facilitates transcytosis across the tumor stroma via Gp60-mediated active transport, thereby promoting drug accumulation in tumor tissues.[42,43] Taken together, our findings indicate that PBSO NPs not only enhance the inhibitory effects of α-Sol on PC cell proliferation, migration, and invasion while inducing apoptosis but also improve the tumor-targeting capability of α-Sol, thereby enhancing its anti-PC efficacy. These results suggest that PBSO NPs represent a safe and effective drug delivery system for PC treatment, with promising potential for clinical translation.

However, despite demonstrating the multiple advantages of PBSO NPs as a drug carrier for α-Sol, this study has certain limitations. First, the current biosafety evaluation system for PBSO NPs remains incomplete, and research on their biological effects in vivo is still in its early stages. Further systematic and in-depth studies, along with large-scale in vitro and in vivo experiments, are required to comprehensively assess their safety. Second, the pharmacokinetic properties of PBSO NPs in vivo have not yet been fully elucidated. Further investigations are needed to clarify their metabolism, distribution, and absorption processes, as well as comparative analyses with other nanocarriers to optimize their delivery performance. Additionally, the antitumor mechanisms of PBSO NPs remain incompletely understood. Whether they possess tumor-suppressing effects beyond the delivery of α-Sol remains unclear, necessitating further exploration of their potential molecular mechanisms. In conclusion, this study confirms that PBSO NPs represent a safe and effective nanoscale delivery system for α-Sol, capable of effectively inhibiting PC progression and holding great promise for clinical translation.

Conclusion

To the best of our knowledge, this study successfully developed PBSO NPs loaded with α-Sol for the first time. PBSO NPs demonstrated good physiological stability and biocompatibility, showing promising potential for clinical applications. In vitro experiments indicated that PBSO NPs could enhance the uptake of the drug by PC cells, inhibit cell viability, invasion, and migration, and promote apoptosis, thereby suppressing tumor cell growth. In vivo experiments further confirmed the significant therapeutic efficacy of PBSO NPs in inhibiting the progression of PC. Additionally, this study found that the anti-PC activity of PBSO NPs was superior to that of free α-Sol and that PBSO NPs could reduce the toxicity of α-Sol to some extent. In summary, this study successfully developed α-Sol-loaded PBSO NPs, which increased the concentration of α-Sol in tumor tissues and exhibited significant anti-PC activity, providing a new therapeutic approach for the treatment of pancreatic cancer in the future.

Funding

Disclosure

The authors declare no conflicts of interest in this work.

References

1. Shi S, Ye L, Jin K. et al. The complement C3a/C3aR pathway is associated with treatment resistance to gemcitabine-based neoadjuvant therapy in pancreatic cancer. *Comput Struct Biotechnol J*. 2024;23:3634–3650. doi:10.1016/j.csbj.2024.09.032
2. Limbu KR, Chhetri RB, Kim S, et al. Targeting sphingosine 1-phosphate and sphingosine kinases in pancreatic cancer: mechanisms and therapeutic potential. *Cancer Cell Int*. 2024;24(1):353. doi:10.1186/s12935-024-03535-7
3. Wu Y, Zhou J, Kou Q, et al. Establishment of a Prognostic Model for Pancreatic Cancer Based on Hypoxia-Related Genes. *Technol Cancer Res Treat*. 2024;23:15330338241288687. doi:10.1177/15330338241288687

4. Song Y, Chen X, Yu X, et al. Dosimetric comparison of multiple SBRT delivery platforms for pancreatic cancer. *Eur J Med Res*. 2024;29(1):533. doi:10.1186/s40001-024-02080-3

5. Qadir R, Umair MB, Tariq UB, et al. Unraveling Pancreatic Cancer: epidemiology, Risk Factors, and Global Trends. *Cureus*. 2024;16(11):e72816. doi:10.7759/cureus.72816

6. Hesami Z, Olfatifar M, Sadeghi A, et al. Global Trend in Pancreatic Cancer Prevalence Rates Through 2040: an Illness-Death Modeling Study. *Cancer Med*. 2024;13(20):e70318. doi:10.1002/cam4.70318

7. Song L, Chen Z, Li Y, et al. Trend and forecast analysis of the changing disease burden of pancreatic cancer attributable to high fasting glucose in China, 1990–2021. *Front Oncol*. 2024;14:1471699. doi:10.3389/fonc.2024.1471699

8. Chen PH, Lee CH, Liaw CC, et al. Metachromin C, a marine-derived natural compound, shows potential in antitumor activity. *Int J Med Sci*. 2024;21(13):2578–2594. doi:10.7150/ijms.101037

9. Yan X, Li M, Chen L, et al. alpha-Solanine inhibits growth and metastatic potential of human colorectal cancer cells. *Oncol Rep*. 2020;43 (5):1387–1396. doi:10.3892/or.2020.7519

10. Luo S, Tian GJ, Yu FX, Wen ZD. A narrative review of the antitumor studies of solanine. *Transl Cancer Res*. 2021;10(3):1578–1582. doi:10.21037/tcr-20-3094

11. Hassan SH, Gul S, Zahra HS, et al. Alpha Solanine: a Novel Natural Bioactive Molecule with Anticancer Effects in Multiple Human Malignancies. *Nutr Cancer*. 2021;73(9):1541–1552. doi:10.1080/01635581.2020.1803932

12. Nandi S, Sikder R, Nag A, et al. Updated aspects of alpha-Solanine as a potential anticancer agent: mechanistic insights and future directions. *Food Sci Nutr*. 2024;12(10):7088–7107. doi:10.1002/fsn3.4221

13. Pan B, Zhong W, Deng Z, et al. Inhibition of prostate cancer growth by solanine requires the suppression of cell cycle proteins and the activation of ROS/P38 signaling pathway. *Cancer Med*. 2016;5(11):3214–3222. doi:10.1002/cam4.916

14. Lv C, Kong H, Dong G, et al. Antitumor efficacy of alpha-solanine against pancreatic cancer in vitro and in vivo. *PLoS One*. 2014;9(2):e87868. doi:10.1371/journal.pone.0087868

15. Wen Z, Huang C, Xu Y, et al. alpha-Solanine inhibits vascular endothelial growth factor expression by down-regulating the ERK1/2-HIF-1alpha and STAT3 signaling pathways. *Eur J Pharmacol*. 2016;771:93–98. doi:10.1016/j.ejphar.2015.12.020

16. Ordóñez-Vásquez A, Aguirre-Arzola V, Garza-Ramos M, Urrutia-Baca V, Suarez-Obando F. Toxicity, teratogenicity and anti-cancer activity of α-solanine: a perspective on anti-cancer potential. *Int J Pharmacol*. 2019;15(3):301–310. doi:10.3923/ijp.2019.301.310

17. Siddique MAB, Brunton N. Food Glycoalkaloids: distribution, structure, cytotoxicity, extraction, and biological activity. In: *Alkaloids-Their Importance in Nature and Human Life*. IntechOpen; 2019.

18. Wang L, Sun QQ, Zhang SJ, et al. Inhibitory effect of alpha-solanine on esophageal carcinoma in vitro. *Exp Ther Med*. 2016;12(3):1525–1530. doi:10.3892/etm.2016.3500

19. Mao L, Gao M, Xue X, et al. Organic-inorganic nanoparticles molecularly imprinted photoelectrochemical sensor for alpha-solanine based on p-type polymer dots and n-CdS heterojunction. *Anal Chim Acta*. 2019;1059:94–102. doi:10.1016/j.aca.2019.01.039

20. Zhao J, Wang L, Zhang H, Liao B, Li Y. Progress of Research in In Situ Smart Hydrogels for Local Antitumor Therapy. *Pharmaceutics*. 2022;14:2028. doi:10.3390/pharmaceutics14102028

21. Manoharan R, Nair CS, Eissa N, et al. Therapeutic potential of Solanum alkaloids with special emphasis on cancer: a comprehensive review, Drug Design. *Development Therapy*. 2024;Volume 18:3063–3074. doi:10.2147/DDDT.S470925

22. Ding Y, Zhang S, Sun Z, et al. Preclinical validation of silibinin/albumin nanoparticles as an applicable system against acute liver injury. *Acta Biomater*. 2022;146:385–395. doi:10.1016/j.actbio.2022.04.021

23. Solanki R, Rostamabadi H, Patel S, Jafari SM. Anticancer nano-delivery systems based on bovine serum albumin nanoparticles: a critical review. *Int J Biol Macromol*. 2021;193(Pt A):528–540. doi:10.1016/j.ijbiomac.2021.10.040

24. Solanki R, Patel K, Patel S. Bovine serum albumin nanoparticles for the efficient delivery of berberine: preparation, characterization and in vitro biological studies, Colloids and Surfaces A. *Physicochem Eng Aspect*. 2021;608:125501. doi:10.1016/j.colsurfa.2020.125501

25. Salehiabar M, Nosrati H, Javani E, et al. Production of biological nanoparticles from bovine serum albumin as controlled release carrier for curcumin delivery. *Int J Biol Macromol*. 2018;115:83–89. doi:10.1016/j.ijbiomac.2018.04.043

26. Huang Y, Hu L, Huang S, et al. Curcumin-loaded galactosylated BSA nanoparticles as targeted drug delivery carriers inhibit hepatocellular carcinoma cell proliferation and migration. *Int J Nanomed*. 2018;13:8309–8323. doi:10.2147/IJN.S184379

27. Bern M, Sand KM, Nilsen J, Sandlie I, Andersen JT. The role of albumin receptors in regulation of albumin homeostasis: implications for drug delivery. *J Control Release*. 2015;211:144–162. doi:10.1016/j.jconrel.2015.06.006

28. Shen X, Liu X, Li T, et al. Recent Advancements in Serum Albumin-Based Nanovehicles Toward Potential Cancer Diagnosis and Therapy. *Front Chem*. 2021;9:746646. doi:10.3389/fchem.2021.746646

29. Alipour B, Veisi Malekshahi Z, Pourjafar F, Faridi-Majidi R, Negahdari B. Anticancer effects of simvastatin-loaded albumin nanoparticles on monolayer and spheroid models of breast cancer. *Biochem Biophys Res Commun*. 2024;734:150591. doi:10.1016/j.bbrc.2024.150591

30. Sleep D. Albumin and its application in drug delivery. *Expert Opin Drug Deliv*. 2015;12:793–812. doi:10.1517/17425247.2015.993313

31. Wang P, Kankala RK, Chen B, et al. Poly-allylamine hydrochloride and fucoidan-based self-assembled polyelectrolyte complex nanoparticles for cancer therapeutics. *J Biomed Mater Res A*. 2019;107:339–347. doi:10.1002/jbm.a.36526

32. Choi JS, Meghani N. Impact of surface modification in BSA nanoparticles for uptake in cancer cells. *Colloids Surf B Biointerfaces*. 2016;145:653–661. doi:10.1016/j.colsurfb.2016.05.050

33. Lian H, Wu J, Hu Y, Guo H. Self-assembled albumin nanoparticles for combination therapy in prostate cancer. *Int J Nanomed*. 2017;12:7777–7787. doi:10.2147/IJN.S144634

34. Hassanzadeh A, Ashrafihelan J, Salehi R, et al. Development and biocompatibility of the injectable collagen/nano-hydroxyapatite scaffolds as in situ forming hydrogel for the hard tissue engineering application. *Artif Cells Nanomed Biotechnol*. 2021;49(1):136–146. doi:10.1080/21691401.2021.1877153

35. Lin T, Zhao P, Jiang Y, et al. Blood-Brain-Barrier-Penetrating Albumin Nanoparticles for Biomimetic Drug Delivery via Albumin-Binding Protein Pathways for Antiglioma Therapy. *ACS Nano*. 2016;10(11):9999–10012. doi:10.1021/acsnano.6b04268

36. Jayachandran P, Ilango S, Suseela V, et al. Green Synthesized Silver Nanoparticle-Loaded Liposome-Based Nanoarchitectonics for Cancer Management: in Vitro Drug Release Analysis. *Biomedicines*. 2023;12(1):11. doi:10.3390/biomedicines11010217

37. Yang J, Liu B, Wang Q, et al. Carboxylated mesoporous silica nanoparticle-nucleic acid chimera conjugate-assisted delivery of siRNA and doxorubicin effectively treat drug-resistant bladder cancer. *Biomed Pharmacother*. 2024;178:117185. doi:10.1016/j.biopha.2024.117185

38. Nakka NMR, Rachamala HK, Angom RS, et al. Dual drug-loaded tumor-targeted polymeric nanoparticles for enhancing therapeutic response in pancreatic ductal adenocarcinoma. *Mater Today Bio*. 2024;28:101199. doi:10.1016/j.mtbio.2024.101199

39. Zhang X, Xu B, Ni J, Xiang Y, He Z. Combined Chemo- and Photothermal Therapies of Non-Small Cell Lung Cancer Using Polydopamine/Au Hollow Nanospheres Loaded with Doxorubicin. *Int J Nanomed*. 2024;19:9597–9612. doi:10.2147/IJN.S473137

40. AbouAitah K, Lojkowski W, Ting SC. Delivery of Natural Agents by Means of Mesoporous Silica Nanospheres as a Promising Anticancer Strategy. *Pharmaceutics*. 2021;14(1):13. doi:10.3390/pharmaceutics13020143

41. Ji YB, Gao SY, Ji CF, Zou X. Induction of apoptosis in HepG2 cells by solanine and Bcl-2 protein. *J Ethnopharmacol*. 2008;115(2):194–202. doi:10.1016/j.jep.2007.09.023

42. Sun H, Lv C, Yang L, et al. Solanine induces mitochondria-mediated apoptosis in human pancreatic cancer cells. *Biomed Res Int*. 2014;2014:805926. doi:10.1155/2014/805926

43. Gu T, Yuan W, Li C, et al. alpha-Solanine Inhibits Proliferation, Invasion, and Migration, and Induces Apoptosis in Human Choriocarcinoma JEG-3 Cells In Vitro and In Vivo. *Toxins*. 2021;14(1):13. doi:10.3390/toxins13030210

44. Kim B, Lee C, Lee ES, Shin BS, Youn YS. Paclitaxel and curcumin co-bound albumin nanoparticles having antitumor potential to pancreatic cancer. *Asian J Pharm Sci*. 2016;11:708–714.

45. Tsai CS, Park JW, Chen LT. Nanovector-based therapies in advanced pancreatic cancer. *J Gastrointest Oncol*. 2011;2(3):185–194. doi:10.3978/j.issn.2078-6891.2011.034

46. Chen B, Zhao Y, Lin Z, et al. Apatinib and gamabufotalin co-loaded lipid/Prussian blue nanoparticles for synergistic therapy to gastric cancer with metastasis. *J Pharm Anal*. 2024;14(5):100904. doi:10.1016/j.jpha.2023.11.011

47. Zhang C, Shi C, Chang P, et al. MRI Directed Magnevist Effective to Study Toxicity of Gd-Doped Mesoporous Carbon Nanoparticles in Mice Model. *Int J Nanomed*. 2023;18:6119–6136. doi:10.2147/IJN.S433213

48. Ding J, Su J, Luo B, Ding L. Preparation and Evaluation of Folate Modified PEG-PLLA Nanoparticles Loaded with Lycorine for Glioma Treatment. *Molecules*. 2024;29:51081. doi:10.3390/molecules29051081

49. Yang Y, Ye T, Shang F, et al. Combined Albumin Polyester Nanocarriers with Docetaxel for Effective Against Lung Cancer in Mice Model. *Int J Nanomed*. 2025;20:2103–2118. doi:10.2147/IJN.S487344

50. de Lazaro I, Mooney DJ. Obstacles and opportunities in a forward vision for cancer nanomedicine. *Nat Mater*. 2021;20(11):1469–1479. doi:10.1038/s41563-021-01047-7

51. Cheng Z, Li M, Dey R, Chen Y. Nanomaterials for cancer therapy: current progress and perspectives. *J Hematol Oncol*. 2021;14(1):85. doi:10.1186/s13045-021-01096-0

52. Wang C, Li F, Zhang T, Yu M, Sun Y. Recent advances in anti-multidrug resistance for nano-drug delivery system. *Drug Deliv*. 2022;29(1):1684–1697. doi:10.1080/10717544.2022.2079771

53. Hao Y, Zhu W, Li J, et al. Sustained release hypoxia-activated prodrug-loaded BSA nanoparticles enhance transarterial chemoembolization against hepatocellular carcinoma. *J Control Release*. 2024;372:155–167. doi:10.1016/j.jconrel.2024.06.026

54. Fang R, Liao Y, Qiu H, et al. Chitosan Oligosaccharide Modified Bovine Serum Albumin Nanoparticles for Improving Oral Bioavailability of Naringenin. *Curr Drug Deliv*. 2024;21(8):1142–1150. doi:10.2174/1567201820666230718143726

55. Gong S, Lang S, Wang Y, et al. pH-Responsive Mesoporous Silica Nanoparticles Loaded with Naringin for Targeted Osteoclast Inhibition and Bone Regeneration. *Int J Nanomed*. 2024;19:6337–6358. doi:10.2147/IJN.S456545

56. Lu Y, Han S, Zheng H, et al. A novel RGDyC/PEG co-modified PAMAM dendrimer-loaded arsenic trioxide of glioma targeting delivery system. *Int J Nanomed*. 2018;13:5937–5952. doi:10.2147/IJN.S175418

57. Ge Z, Ma R, Xu G, et al. Development and In Vitro Release of Isoniazid and Rifampicin-Loaded Bovine Serum Albumin Nanoparticles. *Med Sci Monit*. 2018;24:473–478. doi:10.12659/msm.905581

58. Ahmed SS, Baba MZ, Wahedi U, et al. Oral delivery of solid lipid nanoparticles surface decorated with hyaluronic acid and bovine serum albumin: a novel approach to treat colon cancer through active targeting. *Int J Biol Macromol*. 2024;279:135487. doi:10.1016/j.ijbiomac.2024.135487

59. He Y, Yang M, Yang L, et al. Preparation and anticancer actions of CuET-nanoparticles dispersed by bovine serum albumin. *Colloids Surf B Biointerfaces*. 2023;226:113329. doi:10.1016/j.colsurfb.2023.113329

60. Cai X, Weng Q, Lin J, Chen G, Wang S. Radix Pseudostellariae protein-curcumin nanocomplex: improvement on the stability, cellular uptake and antioxidant activity of curcumin. *Food Chem Toxicol*. 2021;151:112110. doi:10.1016/j.fct.2021.112110

61. Giordano G, Pancione M, Olivieri N, et al. Nano albumin bound-paclitaxel in pancreatic cancer: current evidences and future directions. *World J Gastroenterol*. 2017;23(32):5875–5886. doi:10.3748/wjg.v23.i32.5875

62. Ji Q, Zhu H, Qin Y, et al. GP60 and SPARC as albumin receptors: key targeted sites for the delivery of antitumor drugs. *Front Pharmacol*. 2024;15:1329636. doi:10.3389/fphar.2024.1329636

63. Rossi MK, Gnanamony M, Gondi CS. The 'SPARC' of life: analysis of the role of osteonectin/SPARC in pancreatic cancer (Review. *Int J Oncol*. 2016;48(5):1765–1771. doi:10.3892/ijo.2016.3417

64. Xue G, Jiang H, Song Z, et al. Dual Targeting Biomimetic Carrier-Free Nanosystems for Photo-Chemotherapy of Rheumatoid Arthritis via Macrophage Apoptosis and Re-Polarization. *Adv Sci*. 2025;12(10):e2406877. doi:10.1002/advs.202406877

65. Sanita G, Armanetti P, Silvestri B, et al. Albumin-Modified Melanin-Silica Hybrid Nanoparticles Target Breast Cancer Cells via a SPARC-Dependent Mechanism. *Front Bioeng Biotechnol*. 2020;8:765. doi:10.3389/fbioe.2020.00765

66. Zheng B, Chen Y, Niu L, et al. Modulating the tumoral SPARC content to enhance albumin-based drug delivery for cancer therapy. *J Control Release*. 2024;366:596–610. doi:10.1016/j.jconrel.2023.12.057

67. Lu H, Noorani L, Jiang Y, Du AW, Stenzel MH. Penetration and drug delivery of albumin nanoparticles into pancreatic multicellular tumor spheroids. *J Mater Chem B*. 2017;5(48):9591–9599. doi:10.1039/c7tb02902k

68. Nasrollahi F, Varshosaz J, Khodadadi AA, Lim S, Jahanian-Najafabadi A. Targeted Delivery of Docetaxel by Use of Transferrin/Poly(allylamine hydrochloride)-functionalized Graphene Oxide Nanocarrier. *ACS Appl Mater Interfaces*. 2016;8(21):13282–13293. doi:10.1021/acsami.6b02790

69. Yang R, Yang SG, Shim WS, et al. Lung-specific delivery of paclitaxel by chitosan-modified PLGA nanoparticles via transient formation of microaggregates. *J Pharm Sci*. 2009;98(3):970–984. doi:10.1002/jps.21487

70. Villanueva A, Canete M, Roca AG, et al. The influence of surface functionalization on the enhanced internalization of magnetic nanoparticles in cancer cells. *Nanotechnology.* 2009;20(11):115103. doi:10.1088/0957-4484/20/11/115103

71. Cho EC, Xie J, Wurm PA, Xia Y. Understanding the Role of Surface Charges in Cellular Adsorption versus Internalization by Selectively Removing Gold Nanoparticles on the Cell Surface with a I 2 /KI Etchant. *Nano Lett.* 2009;9(3):1080–1084. doi:10.1021/nl803487r

72. Abdullah HT, Faisal S, Faisal S, et al. Zingiber officinale rhizome extracts mediated ni nanoparticles and its promising biomedical and environmental applications. *BMC Complement Med Ther.* 2023;23(1):349. doi:10.1186/s12906-023-04182-7

73. Gao L, Shay C, Teng Y. Cell death shapes cancer immunity: spotlighting PANoptosis. *J Exp Clin Cancer Res.* 2024;43(1):168. doi:10.1186/s13046-024-03089-6